Raman spectroscopic studies of lithium manganates with spinel structure

2003 J. Phys.: Condens. Matter 15 3151

(http://iopscience.iop.org/0953-8984/15/19/315)

INSTITUTE OF PHYSICS PUBLISHING JOURNAL OF PHYSICS: CONDENSED MATTER

J. Phys.: Condens. Matter **15** (2003) 3151–3162 PII: S0953-8984(03)55422-4

Raman spectroscopic studies of lithium manganates with spinel structure

C M Julien[1] **and M Massot**[2]

[1] Laboratoire des Milieux Désordonnés et Hétérogènes, CNRS-UMR7603, Université Pierre et Marie Curie, case 86, 4 place Jussieu, F-75252 Paris Cedex 05, France
[2] Laboratoire de Physique des Milieux Condensés, CNRS-UMR7602, Université Pierre et Marie Curie, case 77, 4 place Jussieu, F-75252 Paris Cedex 05, France

E-mail: cjul@ccr.jussieu.fr

Received 31 October 2002, in final form 26 March 2003
Published 6 May 2003
Online at stacks.iop.org/JPhysCM/15/3151

Abstract

Raman scattering spectra of a set of lithium manganospinels $Li_{1-x+z}Mn_{2-z}O_4$ with $0 \leqslant x \leqslant 1$ and $0 \leqslant z \leqslant 0.33$ are reported and analysed. Structural changes have been investigated following the evolution of Raman spectra with the concentration of lithium cations. The local structure was characterized as a function of the mean oxidation state of manganese cations. The trigonal distortion of MnO_6 octahedra is evidenced by insertion of lithium ions into the $[B_2]O_4$ spinel framework. A comparison with tetragonal Mn_3O_4 and Fe_3O_4 spinels shows the influence of the Jahn–Teller effect on the Raman features for this class of materials.

1. Introduction

Lithium manganates form an important range of ceramic compounds with very interesting electrical, magnetic and optical properties [1–3]. Goodenough *et al* [4, 5] demonstrated that the $LiMn_2O_4$ spinel framework offers interesting properties as an intercalation compound for positive electrodes in rechargeable lithium batteries. However, the cycling performance of $LiMn_2O_4$ is not satisfactory enough due to the presence of Jahn–Teller (JT) Mn^{3+} ions. Recently, it was found that redox reactions of nonstoichiometric or doped spinels are much better than that of stoichiometric ceramics [6–9]. Because determination of the local structure seems one of the key issues for understanding electrochemical properties, vibrational spectroscopy can be applied to provide information on structural characteristics of $LiMn_2O_4$ oxides.

It is commonly accepted that spinel oxides with the general formula $A[B_2]O_4$ crystallize in either cubic ($Fd3m$ SG) or tetragonal ($I4_1/amd$ SG) structures. It is the presence of JT ions in the octahedral sites of the oxygen close-packed arrangement of the structure that is responsible for the octahedral deformation and, in turn, for the tetragonal distortion. Previous literature

devoted to the spinel oxides dealt essentially with the infrared spectra of $A^{II}[B^{III}]_2O_4$ materials [10–14]. There are limited works dedicated to the study of Raman spectra of the cubic spinel $LiMn_2O_4$ [15–18] and the tetragonally distorted Mn_3O_4 [12].

To quantify the nature and amplitude of disorder in synthetic $LiMn_2O_4$ spinels from vibrational features, a systematic analysis of Raman spectra was carried out on a set of $Li_{1-x+z}Mn_{2-z}O_4$ oxides with $0 \leqslant x \leqslant 1$ and $0 \leqslant z \leqslant 0.33$. The Raman features are discussed in light of the different mean oxidation states of Mn ions.

2. Experiment

The λ-$LiMn_2O_4$ and lithium-rich $Li_{1+z}Mn_{2-z}O_4$ spinel oxides were prepared using the melt-impregnation method by mixing a fine powder of LiOH and MnO_2 with 7 mol% excess of LiOH to compensate for the loss of lithium during heat treatment [15]. The mixtures were ground inside a dry box filled with argon to prevent carbonate formation. The mixtures were then packed in a ceramic boat and heat treated at 470 °C for 4 h. At this temperature LiOH melts and uniformly coats the MnO_2 grains. The products were then ground to fine powders and heat treated at 750 °C for 12 h under flow of oxygen. The final products were cooled to room temperature under a continuous flow of oxygen. The delithiated λ-MnO_2 sample was prepared by Hunter's method, which consists of the Li extraction by acid digestion [19]. Tetragonal $Li_2Mn_2O_4$ was chemically synthesized from reaction of λ-$LiMn_2O_4$ with LiI in heated acetone solution according to the method described by Tarascon and Guyomard [20]. The partially delithiated spinel $Li_{0.5}Mn_2O_4$ sample was obtained from electrochemical extraction of Li^+ ions from λ-$LiMn_2O_4$. Microcrystalline Mn_3O_4 and Fe_3O_4 were available as commercial oxide powders (Aldrich purum grade). The structure of the samples was characterized by x-ray powder diffraction (XRPD) using a diffractometer (Philips model PW1830) with nickel-filtered Cu Kα radiation ($\lambda = 1.5406$ Å). The diffraction patterns were taken in the range of $5° < 2\theta < 80°$ using step scans.

Raman scattering spectra were taken between 4 and 1200 cm^{-1} at room temperature in a quasi-backscattering configuration. A double monochromator (Jobin–Yvon model U1000) with holographic gratings and a computer-controlled photon-counting system was used. The laser light source was the 514.5 nm line radiation from a Spectra-Physics 2020 argon-ion laser. To have a high signal–noise ratio, each RS spectrum is the average of 12 successive scans obtained at a spectral resolution of 2 cm^{-1}. The frequency stability and the accuracy of the apparatus was checked by recording the Raman spectrum of silicon. To avoid sample photodecomposition or denaturation, RS spectra were recorded using a low excitation power of 10 mW. An increase in lattice temperature generally results in a shift of Raman peak wavenumber up to the formation of Mn_3O_4 oxide. All powders were pelletized to obtain a mirror-like surface sample for Raman analysis.

Raman spectra were fitted using the GRAM/386 software from Galatic Industries Co. The curve analysis is based on the original algorithm of non-linear peak fitting described by Marquardt and known as the Levenberg–Marquardt method [21]. The fitting calculations were done assuming a linear baseline for the spectra and that all the Raman lines introduced in the fit have a Lorentz lineshape.

3. Structure and group theory analysis of spinels

The spinel structures contain a three-dimensional interstitial space for Li-ion transport in the cubic-close-packed (ccp) system $Li_xMn_{2-y}O_4$ ($0 \leqslant x \leqslant 4/3, 0 \leqslant y \leqslant 1/3$) [1]. A

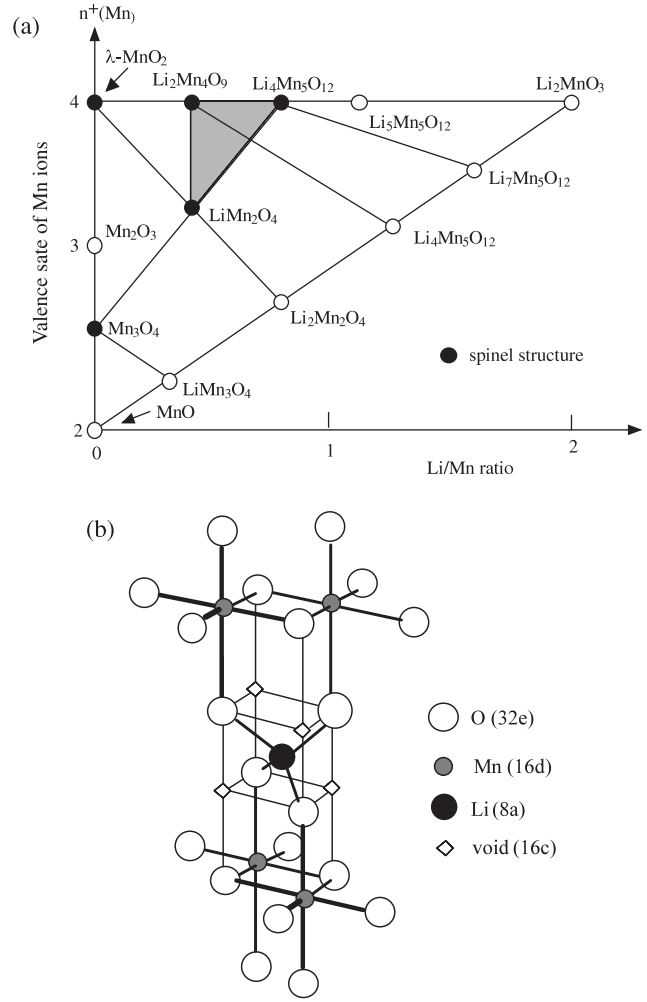

Figure 1. (a) Phase diagram of lithium manganese oxides. (b) Schematic representation of the spinel structure of $LiMn_2O_4$.

representation of the Li–Mn–O phase diagram highlighting the positions of spinel compositions is shown in figure 1(a); a scheme of the $LiMn_2O_4$ spinel structure is presented in figure 1(b). The approximately ccp array of oxide ions incorporates MnO_6 octahedra sharing two opposite corners with LiO_4 tetrahedra. It is commonly accepted that normal $A[B_2]O_4$ spinel exhibits a cubic structure, with space group $Fd3m$ (O_h^7) with $Z = 8$. In this structure, the anions form a nearly ideal close-packed pseudo-face-centred-cubic sublattice surrounded by tetrahedral and octahedral sites. Cations occupy only $1/8$ of the tetrahedrally coordinated sites (8a Wyckoff position) and $1/2$ of the octahedrally coordinated sites (16d Wyckoff position). In an ideal $A[B_2]O_4$ spinel structure, A atoms are located on tetrahedral sites of T_d symmetry and B atoms on octahedral sites of D_{3d} symmetry, whereas oxygen atoms occupy C_{3v} sites (32e Wyckoff position) [22]. To complete the description of the anion position, an additional parameter, generally labelled u and known in oxide spinels as the internal oxygen parameter, is introduced. In $LiMn_2O_4$ spinel, u is 0.263 when the origin of the unit cell is taken at the centre of inversion.

Table 1. Factor group analysis of the $LiMn_2O_4$ spinel structure (O_h^7 space group).

Atom	Site	Irreducible representation
Li	T_d	$F_{2g} \oplus F_{1u}$
Mn	D_{3d}	$2F_{1u} \oplus A_{2u} \oplus E_u \oplus F_{2u}$
O	C_{2v}	$A_{1g} \oplus E_g \oplus 2F_{2g} \oplus 2F_{1u} \oplus F_{1g} \oplus A_{2u} \oplus E_u \oplus F_{2u}$
Total		$A_{1g} \oplus E_g \oplus 3F_{2g} \oplus 5F_{1u} \oplus F_{1g} \oplus 2A_{2u} \oplus 2E_u \oplus 2F_{2u}$
Acoustic		F_{1u}
Raman		$A_{1g} \oplus E_g \oplus 3F_{2g}$
Infrared		$4F_{1u}$

For a regular octahedral MnO_6^{2-} anion with O_h symmetry, three stretching modes $\nu_1(A_{1g})$, $\nu_2(E_g)$ and $\nu_3(F_{1u})$, and three bending modes $\nu_4(F_{1u})$, $\nu_5(F_{2g})$ and $\nu_6(F_{2u})$, are allowed, where ν_1, ν_2 and ν_5 are Raman-active modes, ν_3 and ν_4 are infrared-active modes and ν_6 is a silent mode. In general, the order of the stretching frequencies is $\nu_1 > \nu_3 > \nu_2$ or $\nu_3 > \nu_1 > \nu_2$, while the order of bending frequencies is $\nu_4 > \nu_5 > \nu_6$ [23]. Since in the $LiMn_2O_4$ spinel structure, the MnO_6 octahedron is slightly distorted due to the presence of the JT Mn^{3+} ion, the vibrational modes should be analysed by using the corresponding correlation method (table 1). The whole cubic cell of the spinel structure contains 56 atoms and is largely redundant as regards determining the number of vibrations of the lattice from group theoretical considerations, since only two octants of the cell, which lie along the main body diagonal, are really different. Taking the reduced cell, which contains 14 atoms and is equivalent to the smallest Bravais cell, the total number of vibration modes at the centre of the Brillouin zone can be described using the method of site group analysis by Rousseau *et al* [24]. The distribution of the degree of freedom in an irreducible representation of the O_h^7 factor group was calculated and represented in table 1. The irreducible representation of optical allowed modes for the $LiMn_2O_4$ spinel is

$$\Gamma(LiMn_2O_4) = A_{1g}(R) \oplus E_g(R) \oplus 3F_{2g}(R) \oplus 4F_{1u}(\mathrm{ir}), \tag{1}$$

where R(ir) denotes Raman (infrared) activity and the remaining modes (table 1) are silent. Recently, Ammundsen *et al* [16] have calculated the lattice dynamics of lithium manganese oxides using atomistic modelling methods, while Sinha and Gupta [17] have estimated the zone-centre phonons by applying the de Launey angular force constant model.

4. Spectroscopic results

4.1. λ-$LiMn_2O_4$ spinel

Figure 2 shows the Raman spectra of λ-$LiMn_2O_4$ spinel and its delithiated products $Li_{0.5}Mn_2O_4$ and λ-MnO_2 in the spectral region between 100–800 cm^{-1}. A common feature of these spectra is the presence of a strong band around 600 cm^{-1} and a group of bands between 200–500 cm^{-1} with weaker intensity. In spinel oxides and in other manganese oxides energies of ∼600–650 cm^{-1} are characteristic of vibrations involving the motion of oxygen atoms inside the octahedral unit MnO_6 [25]. The assignment of modes observed in the RS spectrum of λ-$LiMn_2O_4$ spinel has been reported previously [15–17]. The Raman band located at about 625 cm^{-1} is viewed as the symmetric Mn–O stretching vibration of MnO_6 groups. This high-wavenumber band is assigned to the A_{1g} species in the O_h^7 spectroscopic symmetry. Its broadness is related to the cation–anion bond lengths and polyhedral distortion occurring in $LiMn_2O_4$. As the manganese ions of the spinel structure exhibit a charge disproportionation such as $LiMn^{3+}Mn^{4+}O_4$, there are isotropic $Mn^{4+}O_6$ octahedra and locally distorted $Mn^{3+}O_6$

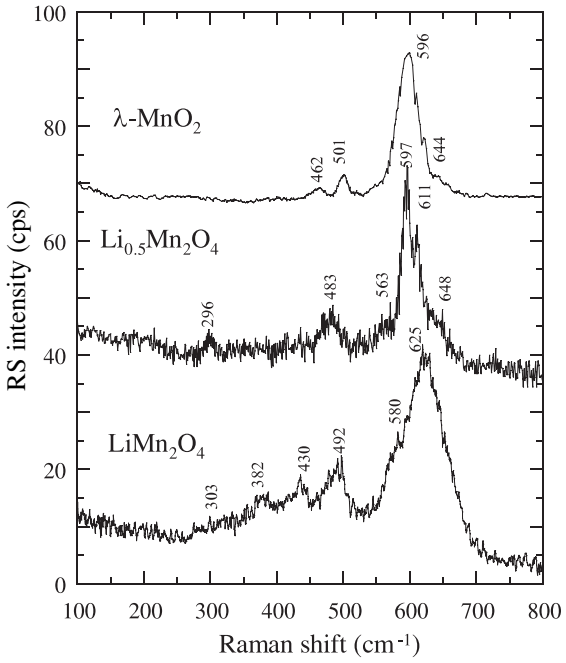

Figure 2. Raman spectra of $Li_{1-x+\partial}[Mn_{2-\partial}]O_4$ cubic spinels with $\partial = 0$ and $0 \leqslant x \leqslant 1$ (bottom) λ-$LiMn_2O_4$, (middle) $Li_{0.5}Mn_2O_4$ and (top) λ-MnO_2.

octahedra due to the JT effect. Thus, we expect to observe stretching vibrations of MnO_6^{9-} and MnO_6^{8-} octahedra which provide the broadness of the A_{1g} mode. The shoulder peak at 580 cm^{-1} of the $F_{2g}^{(1)}$ mode in this region is not well separated because of its low intensity. In the localized vibration approach, it is speculated that the intensity of the Raman shoulder is closely related to the manganese average oxidation state in the spinel phase. As the intensity of this shoulder is very sensitive to the lithium stoichiometry, it is suggested that its character originates mainly from the vibration of Mn^{IV}–O bonding. The RS peak with medium intensity located at 483 cm^{-1} has the $F_{2g}^{(2)}$ symmetry, while the weak bands located at 426 and 382 cm^{-1} have the E_g and $F_{2g}^{(3)}$ symmetry, respectively. The $F_{2g}^{(3)}$ mode is related to the Li–O motion, i.e. connected to the tetrahedral cation movements. The low-wavenumber band at 300 cm^{-1} is a unexpected mode, which could be Raman-active due to the cationic disorder that induces a breakdown of the translation symmetry. It can be stated that in the ideal cubic spinel $LiMn_2O_4$, the Mn^{3+} and Mn^{4+} cations are considered as crystallographically equivalent (16d sites) in agreement with XRD data; therefore, occupation probabilities of 0.5 must be affected for each cation in the 16d position. Hence, a loss of translation invariance certainly occurs, due to local lattice distortions around the Mn^{3+} cations which exhibit a JT effect and have higher ionic radii than Mn^{4+} ions. As a result, a breakdown in the Raman and IR selection rules is expected, which may explain the observation of broad bands (somewhat disordered) and the fact that more vibrational modes than expected are observed in cubic $LiMn_2O_4$. The weak Raman scattering efficiency is attributed to the electronic properties of $LiMn_2O_4$. It is a fact that $Li[Mn^{3+}Mn^{4+}]O_4$ is a small-polaron semiconductor, in which the electron hopping occurs between the two oxidation states of manganese ions [26]. An increase in conductivity, i.e. high concentration of carriers, reduces the optical skin depth (strong optical absorbance)

Table 2. Raman data of Li–Mn–O samples.

Sample	Wavenumber (cm^{-1})							
λ-$LiMn_2O_4$	—	303	382	430	492	580	625	—
$Li_{0.5}Mn_2O_4$	—	296	—	483	563	597	611	648
λ-MnO_2	—	—	—	462	501	596	—	644
$Li_{1.18}Mn_{1.82}O_4$	—	298	374	—	485	590	628	669
$Li_{1.24}Mn_{1.76}O_4$	—	300	375	430	485	590	630	647
$Li_{1.33}Mn_{1.67}O_4$	—	304	376	434	491	600	634	653
$Li_2Mn_2O_4$	258	279	401	—	468	—	608	—

of the incident laser beam in the visible region, resulting in a decrease in Raman scattering intensity. Raman data of Li–Mn–O samples are gathered in table 2.

4.2. λ-MnO_2 spinel

The extraction of Li^+ ions from the λ-$LiMn_2O_4$ spinel framework results in the λ-Mn_2O_4 phase ($\square_{tetr}[Mn_2]_{oct}O_4$ spinel notation), which also has a cubic structure ($Fd3m$ SG). Analysis of the vibrational spectra of spinel λ-MnO_2 can be made by classical factor group theory using the O_h^7 spectroscopic symmetry. The total irreducible representation for the vibrational modes of λ-MnO_2 reduces to

$$\Gamma(\lambda\text{-}Mn_2O_4) = A_{1g}(R) \oplus E_g(R) \oplus 2F_{2g}(R) \oplus 3F_{1u}(\text{ir}). \tag{2}$$

Four optic modes are Raman-active vibrations ($A_{1g} \oplus E_g \oplus 2F_{2g}$). The vibrational modes of the Raman-allowed phonons result in the loss of $F_{2g} \oplus F_{1u}$ phonons with the removal of lithium from the spinel λ-$LiMn_2O_4$. The F_{2g} Raman-active phonons become modes of oxygen ions only, along with the E_g mode [16]. The dominant feature of the Raman spectrum of λ-MnO_2 (figure 2) is the strong band centred at 596 cm^{-1} attributed to the A_{1g} species. This is the stretching mode of MnO_6 octahedra in λ-MnO_2. Three weak bands appear at 461, 501 and 646 cm^{-1}. To determine the variation in spinel spectral features, calculations of lattice vibrational modes of λ-MnO_2 have shown that the wavenumbers of the E_g and F_{2g} modes are expected to increase, while the wavenumber of the A_{1g} mode is predicted to decrease. Our experimental data for λ-MnO_2 support these predictions. The peak position of the A_{1g} mode shifts toward the low-frequency side by 27 cm^{-1}, while the $F_{2g}^{(1)}$ mode is displaced by 31 cm^{-1} towards high wavenumbers. As predicted by factor group analysis, the $F_{2g}^{(3)}$ mode at 382 cm^{-1} is absent in the Raman spectrum of the fully delithiated λ-MnO_2 phase.

4.3. $Li_{0.5}Mn_2O_4$ delithiated spinel

The low-wavenumber Raman features of the delithiated $Li_{0.5}Mn_2O_4$ phase (figure 2) display almost the same shape as the λ-$LiMn_2O_4$ spinel. However, in the high-wavenumber region, above 500 cm^{-1}, the bands at 563, 597, 611 and 648 cm^{-1} are diagnostic of the T_d^2 spectroscopic symmetry. For intermediate compositions such as the particular $Li_{0.5}Mn_2O_4$ every second lithium tetrahedral site is vacant, producing an ordered Li configuration. Thus the $Li_{0.5}Mn_2O_4$ spinel lattice can be modelled in the $F\bar{4}3m$ space group, which is a lower symmetry subgroup of $Fd3m$. The calculation for $Li_{0.5}Mn_2O_4$ shows phonons which derived from Raman-active modes of the $LiMn_2O_4$ and λ-MnO_2 phases. The total irreducible representation for the vibrational modes of the $Li_{0.5}Mn_2O_4$ phase is

$$\Gamma(Li_{0.5}Mn_2O_4) = 3A_1(R) \oplus 3E(R) \oplus 3F_1(R) \oplus 6F_2(R, \text{ir}). \tag{3}$$

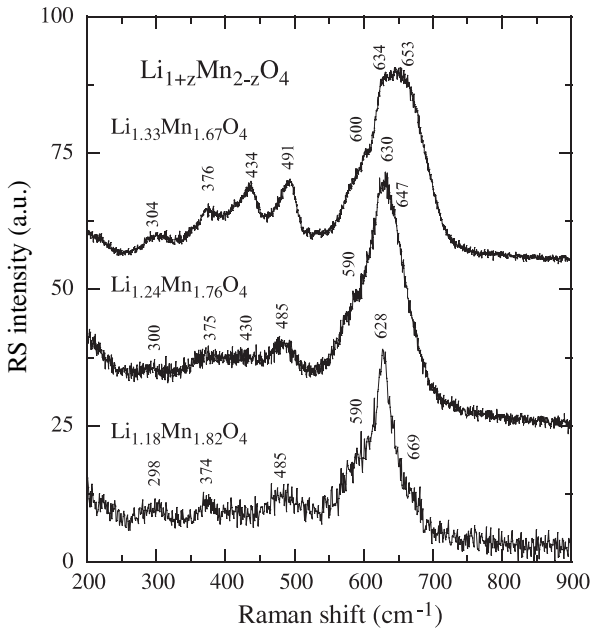

Figure 3. Raman spectra of $Li_{1-x+\partial}[Mn_{2-\partial}]O_4$ cubic spinels with $x = 0$ and $0.00 \leqslant \partial \leqslant 0.33$. (Bottom) $Li_{1.18}Mn_{1.82}O_4$, (middle) $Li_{1.24}Mn_{1.76}O_4$ and (top) $Li_{1.33}Mn_{1.67}O_4$.

The two most intense bands at 597 and 611 cm^{-1} are assigned to the modes of A_1 and F_2 symmetry derived from the Raman-active modes A_{1g} and $F_{2g}^{(3)}$ modes under O_h^7 spectroscopic group [16]. The band at 483 cm^{-1} is attributed to the F_2 mode which is related to the $F_{2g}^{(2)}$ mode under O_h^7 spectroscopic group.

4.4. Li-rich $Li_{1+z}Mn_{2-z}O_4$ spinels

Figure 3 shows the RS spectra of $Li_{1.18}Mn_{1.82}O_4$, $Li_{1.24}Mn_{1.76}O_4$ and $Li_{1.33}Mn_{1.67}O_4$ lithium-rich oxides, which have the λ-$LiMn_2O_4$ spinel-like structure. The general trend of the RS spectrum of $Li_{1.18}Mn_{1.82}O_4$, which shows a resemblance with that of λ-$LiMn_2O_4$, is the frequency shift of the $F_{2g}^{(1)}$ and A_{1g} mode and the appearance of a new band at high wavenumber. The RS spectra of the $Li_{1+z}Mn_{2-z}O_4$ spinels display a dominant band centred at 630–650 cm^{-1} that corresponds to the Mn–O stretching vibrations. A close examination leads to two components at 647 and 630 cm^{-1} for $Li_{1.24}Mn_{1.76}O_4$, which are shifted to 653 and 634 cm^{-1}, respectively, for $Li_{1.33}Mn_{1.67}O_4$. As the series of the spinel-type lithium manganese oxides $Li_{1+z}Mn_{2-z}O_4$, or $(Li)_{tetr}[Li_zMn_{2-z}]_{oct}O_4$ in spinel notation, contain Li ions in vacant 16d octahedral sites, we can expect a slight tetragonal distortion. The net effect could be a breakdown of the translation symmetry because of the random distribution of the metal ions on the octahedral sites; consequently, a common feature of these RS spectra is the presence of some bands in addition to the Raman-active mode vibrations allowed by the space group theory for an ideal spinel structure. It should also be noted that the emergence of some IR-active F_{1u} modes in the first-order RS spectra was explained by the same lowering in the symmetry caused by the disordering in the cation sublattice [11]. Comparing the RS features with those of λ-$LiMn_2O_4$, the increasing stretching frequency is attributed to the shortness of the Mn–O bonds in $Li_{1.33}Mn_{1.67}O_4$. Due to the presence of the Li atoms in octahedral holes,

Table 3. Correlation between room-temperature phase (cubic) and low-temperature phase (orthorhombic) of $LiMn_2O_4$, and $Li_2Mn_2O_4$ (tetragonal).

Phase space group	Spinel $Fd3m$	Tetragonal $I4_1/amd$	Orthorhombic $Fddd$
Atom occupancy	1(Li): 8a	2(Li): 8a, 16c	4(Li): 8a, 16e, 16f, 32h
	1(Mn): 16d	1(Mn): 16d	1(Mn): 16d
			1(Mn): 32h
	1(O): 32e	1(O): 32e	9(O): 32h
Vibrational modes	A_{1g}	A_{1g}	A_g
	E_g	$A_{1g} \oplus B_{1g}$	$A_g + B_{1g}$
	F_{1g}	$A_{2g} \oplus E_g$	$B_{1g} + B_{2g} + B_{3g}$
	$3F_{2g}$	$3(B_{2g} \oplus E_g)$	$3(A_g + B_{2g} + B_{3g})$
	$2A_{2u}$	$2B_{1u}$	$2B_{1u}$
	$2E_u$	$2(A_{1u} \oplus B_{1u})$	$2(A_u + B_{1u})$
	$5F_{1u}$	$5(A_{2u} \oplus E_u)$	$5(B_{1u} + B_{2u} + B_{3u})$
	$2F_{2u}$	$2(B_{2u} \oplus E_u)$	$2(A_u + B_{2u} + B_{3u})$

the frequency of the A_{1g} stretching mode is influenced by bonding and repulsion effects of the tetrahedrally coordinated metal ions [11]. Furthermore, this would be consistent with the fact that the spectral features in the low-frequency domain of the RS spectrum of $Li_{1.33}Mn_{1.67}O_4$ are not markedly different from those of $LiMn_2O_4$, where, of course, a significant increase of the peak located at 300 cm^{-1} occurs. It was speculated that this Raman band is partly related to the stretching vibration of Li ions in octahedral coordination [2]. As this peak grows upon lithium occupancy in 16d sites, it is also partly associated with the presence of Mn^{IV}–O bonding.

4.5. $Li_2Mn_2O_4$ rock-salt phase

When Li^+ ions are inserted into the λ-$LiMn_2O_4$ spinel framework, it transforms to the $Li_2Mn_2O_4$ rock-salt phase that has a tetragonal structure with $I4_1/amd$ (D_{4h}^{19}) space group [27]. This is attributed to the inserted lithium atoms occupying the octahedral 16c sites and the presence of Mn^{3+} JT ions. In this structure Mn^{3+} ions occupy the 8d sites and O^{2-} anions are located at the 16h sites. In order to identify the Raman-active phonons in the tetragonal phase, we correlate the irreducible representation $O_h \rightarrow D_{4h}$ given by table 3. Thus after subtracting the acoustic modes, the optically active modes for $Li_2Mn_2O_4$ are given by

$$\Gamma(Li_2Mn_2O_4) = 2A_{1g}(R) \oplus 4E_g(R) \oplus B_{1g}(R) \oplus 3B_{2g}(R) \oplus 4A_{2u}(\mathrm{ir}) \oplus 6E_u(\mathrm{ir}), \qquad (4)$$

Figure 4 shows the Raman spectra of Fe_2O_4, Mn_2O_4 and $Li_2Mn_2O_4$ tetragonal spinels in the spectral region between 150–900 cm^{-1}. All the spectra show common features: a strong peak at 620–660 cm^{-1} and a group of bands between 200–600 cm^{-1}. Less intense bands are detectable toward the low-wavenumber side in each sample. Referring to the spectrum of Fe_3O_4, we assigned the clearly detectable Raman peaks with species of the normal spinel. In this study, a comparison is done between vibrational features of $Li_2Mn_2O_4$ and those of spinel lattices. The magnetite, Fe_3O_4, and the hausmannite, Mn_3O_4, crystallize with a tetragonal spinel-like lattice and can be expressed in spinel notation as $Fe[Fe_2]O_4$ or $Mn[Mn_2]O_4$. The RS spectra of these spinels are dominated by a strong band attributed to the A_{1g} species at about 674 and 654 cm^{-1}, respectively. The five Raman bands are assigned to the irreducible representation for a spinel lattice in the order of decreasing wavenumber: $A_{1g} > F_{2g}^{(1)} > F_{2g}^{(2)} > E_g > F_{2g}^{(3)}$.

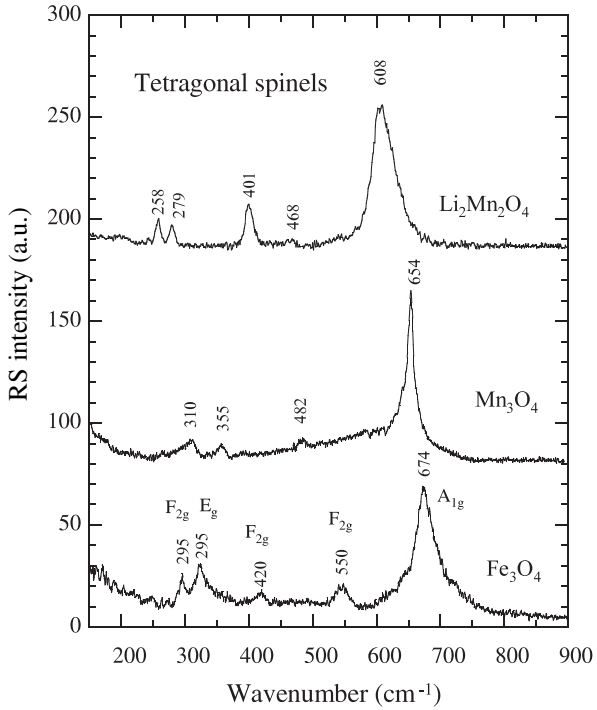

Figure 4. Raman spectra of tetragonal spinel structures. (Top) $Li_2Mn_2O_4$, (middle) Mn_3O_4 and (bottom) Fe_3O_4.

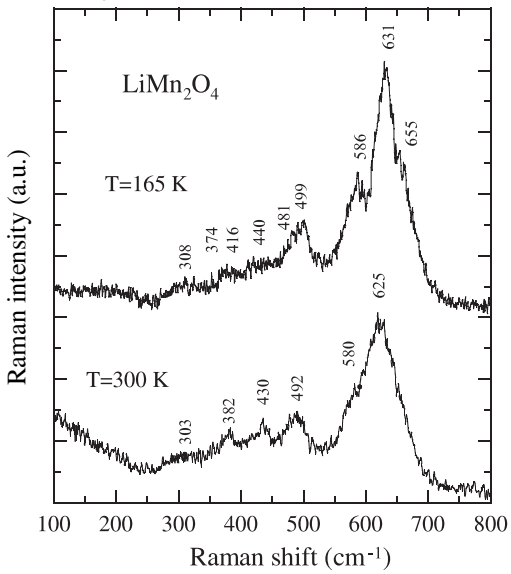

Figure 5. Raman spectra of the $LiMn_2O_4$ orthorhombic phase recorded at 165 K.

4.6. Low-temperature phase

We now consider the temperature behaviour of the observed Raman spectrum of $LiMn_2O_4$ recorded at 165 K. As is seen from figure 5, the number and positions of the RS bands

are temperature-dependent. The net effect of the lowering temperature of λ-$LiMn_2O_4$ is the first-order phase transition from cubic to orthorhombic structure, which occurs around 290 K [28, 29]. The orthorhombic form ($Fddd$ SG), which is attributed to a charge ordering transition, is a superstructure of the cubic phase including 72 Li, 144 Mn and 288 O atoms distributed onto 18 different crystallographic sites [30]. The existence of a large elementary cell suggests the lowering of the spectroscopic symmetry from O_h^7 to D_{2h}^{24}. As this latter lattice is considered as a lower symmetry, we expect an increasing number of phonons. The vibrational modes assignment of the orthorhombic phase can be derived from those of the spinel phase λ-$LiMn_2O_4$ using the correlation of the irreducible representation $O_h \rightarrow D_{2h}$, as shown in table 3. The total irreducible representation for the orthorhombic phase is given by

$$\Gamma_3 = 5A_g(R) \oplus 2B_{1g}(R) \oplus 4B_{2g}(R) \oplus 4B_{3g}(R) \oplus 4A_u(in) \oplus 8B_{1u}(\mathrm{ir}) \oplus 6B_{2u}(\mathrm{ir}) \oplus 6B_{3u}(\mathrm{ir}), \quad (5)$$

for which a huge number of vibrations are expected to be 15 Raman- and 20 IR-active modes. Consequently, the phonon spectrum should become much more structured below the transition temperature, confirming that the crystal structure is more distorted.

The temperature dependence of the infrared features of $LiMn_2O_4$ has been recently investigated by Paolone *et al* [30] while, to our knowledge, no Raman spectrum has been studied in the low-temperature range. As expected, the low-temperature RS spectrum (figure 5) displays a global band shift toward the high-wavenumber side due to the lattice freezing at 165 K that shrinks the MnO_6 skeleton. In addition, we observe several changes in the spectral features as follows.

(i) The Raman scattering efficiency increases due to the lowering of the electrical conductivity, i.e. the electron hop freezing below 300 K.
(ii) The phonon spectrum appears to be much more structured than the room-temperature spectrum due to the orthorhombic D_{2h}^{24} symmetry at temperatures lower than 280 K.
(iii) The bandwidth of the phonon lines becomes narrow.
(iv) The high-wavenumber phonon lines at 481 and 631 cm^{-1} split and new phonons appear in the high-wavenumber side at 499 and 655 cm^{-1}, respectively.
(v) The F_{2g} mode at 586 cm^{-1} (shoulder at 300 K) has changed, giving rise to a well-resolved band.
(vi) A broad band is recorded in the low-wavenumber region which is attributed to external modes.

4.7. Influence of the mean oxidation state of Mn cations

The structural changes of $Li_{1-x+z}Mn_{2-z}O_4$ spinels can be analysed following the evolution of Raman spectra with the concentration of lithium cations and the mean oxidation state of manganese cations denoted by n^+ (Mn). The gradual changes in the energy of the Raman modes are consistent with XRD data for the $Li_{1-x+z}Mn_{2-z}O_4$ solid solution. A comparison between information obtained by Raman and x-ray diffraction is shown in figure 6(a), where the Raman shift for the high-energy A_{1g} mode and the cell volume are plotted as a function of the Li content. An increase of the cell volume leads to a reduction of the bond force constants and to the observed softening of the Raman frequencies. Nevertheless, one can notice the non-linear dependence of the energy with Li content. Figure 6(b) shows the evolution of the high-wavenumber A_{1g} mode as a function of the mean oxidation state of Mn cations for various spinels. A correlation between the n^+ (Mn) value and the Raman peak shift can be shown; by increasing the mean oxidation state the phonon energy progressively decreases. Furthermore, the peak energy decreases with the decrease of the trigonal distortion represented by the c/a

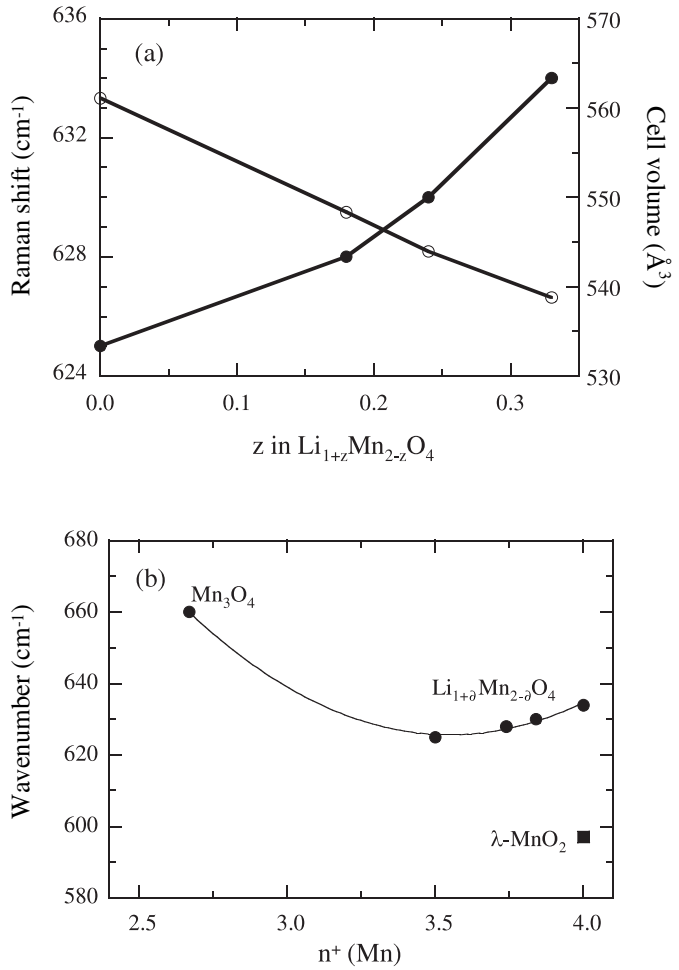

Figure 6. (a) Raman shift of mode A_{1g} (full circles) and cell volume evolution (open circles) along the solid solution $Li_{1+\partial}Mn_{2-\partial}O_4$. (b) Variation of the A_{1g} mode as a function of the mean oxidation state of Mn ions in manganese spinels.

ratio from 654 cm^{-1} in Mn_3O_4 ($c/a = 1.64$) to 625 cm^{-1} in $LiMn_2O_4$ ($c/a = 1.00$). This behaviour proves the indirect influence of the A-type ion on this mode of the octahedral units of the spinel phase. As the metal–oxygen bond length is related to the ionic radius of the Mn ion, this assumption suggests that a direct relation exists between a metal–oxygen bond length and its Raman stretching frequency. The high-energy peak, probably the total-symmetric A_{1g} mode derived from the MnO_6 vibrational units, seems closely related to the static cooperative JT distortion that characterizes these spinels, as shown by the dependence of intensity position and bandwidth of this mode with the cation substitution.

5. Conclusion

Structural properties of Li–Mn–O compounds have been studied by Raman scattering spectroscopy. The vibrational modes of a set of $Li_{1-x+z}Mn_{2-z}O_4$ cubic spinels with $0 \leqslant x \leqslant 1$

and $0 \leqslant \partial \leqslant 0.33$ have been reported and analysed. Structural changes have been analysed following the evolution of Raman spectra with the concentration of lithium cations. The Raman features of the orthorhombic phase of $LiMn_2O_4$ (at 165 K) has been reported for the first time showing the phonon spectrum in agreement with group theory for the $Fddd$ symmetry. The trigonal distortion of MnO_6 octahedra has been shown by insertion of lithium ions into the $[B_2]O_4$ spinel framework to form $Li_2Mn_2O_4$. A comparison with Mn_3O_4 and Fe_3O_4 tetragonal spinels has shown the influence of the JT effect on the Raman features for this class of materials. The local structure of $Li_{1-x+\partial}Mn_{2-\partial}O_4$ has been correlated with the mean oxidation state of manganese cations.

References

[1] Ohzuku T, Kitagawa M and Hirai T 1990 *J. Electrochem. Soc.* **137** 769
[2] Julien C 2001 *NATO ASI Series* **3-85** 309
[3] Rodriguez-Carjaval J, Rousse G, Masquelier C and Hervieu M 1998 *Phys. Rev. Lett.* **81** 4660
[4] Thackeray M M, David W I F, Bruce P G and Goodenough J B 1983 *Mater. Res. Bull.* **18** 461
[5] Thackeray M M, Johnson P J, DePicciotto L A, Bruce P G and Goodenough J B 1984 *Mater. Res. Bull.* **19** 179
[6] Gummow R J, DeKock A and Thackeray M M 1994 *Solid State Ion.* **69** 59
[7] Pistoia G, Antonini A, Rosati R and Bellitto C 1996 *J. Electroanal. Chem.* **410** 115
[8] Hayashi N, Ikuta H and Wakihara M 1999 *J. Electrochem. Soc.* **146** 1351
[9] Julien C, Ziolkiewicz S, Lemal M and Massot M 2001 *J. Mater. Chem.* **11** 1837
[10] Preudhomme J and Tarte P 1971 *Spectrochim. Acta* A **27** 1817
[11] Lutz H D, Becker W, Müller B and Jung M J 1989 *J. Raman Spectrosc.* **20** 99
[12] Lutz H D, Müller B and Steiner H J 1991 *J. Solid State Chem.* **90** 54
[13] Allen G C and Paul M 1995 *Appl. Spectrosc.* **49** 451
[14] Richardson T J and Ross P N Jr 1996 *Mater. Res. Bull.* **31** 935
[15] Julien C, Rougier A, Haro-Poniatowski E and Nazri G A 1998 *Mol. Cryst. Liq. Cryst.* **311** 81
[16] Ammundsen B, Burns G R, Islam M S, Kanoh H and Rozière J 1999 *J. Phys. Chem.* B **103** 5175
[17] Sinha M M and Gupta H C 2002 *Physica* B **316/317** 166
[18] Huang W and Frech R 1999 *J. Power Sources* **81/82** 616
[19] Hunter J C 1981 *J. Solid State Chem.* **39** 142
[20] Tarascon J M and Guyomard D 1991 *J. Electrochem. Soc.* **138** 2864
[21] Marquardt D W 1963 *J. Soc. Ind. Appl. Math.* **11** 431
[22] Wyckoff R W G 1965 *Crystal Structures* vol 3, 2nd edn (New York: Interscience)
[23] White W B and DeAngelis B A 1967 *Spectrochim. Acta* A **23** 985
[24] Rousseau D L, Bauman R P and Porto S P S 1981 *J. Raman Spectrosc.* **10** 253
[25] Julien C, Massot M, Rangan S, Lemal M and Guyomard D 2002 *J. Raman Spectrosc.* **33** 223
[26] Goodenough J B, Manthiram A and Wnetrzewski B 1993 *J. Power Sources* **43/44** 269
[27] David W I F, Thackeray M M, DePicciotto L A and Goodenough J B 1987 *J. Solid State Chem.* **67** 316
[28] Yamada A 1996 *J. Solid State Chem.* **122** 160
[29] Hayakawa H, Takada T, Enoki H and Akiba E 1998 *J. Mater. Sci. Lett.* **17** 811
[30] Paolone A, Roy P, Rousse G, Masquelier C and Rodriguez-Carvajal J 1999 *Solid State Commun.* **111** 453